On the origin of the quasi-perpendicular ion foreshock: Full-particle simulations

Philippe Savoini, Bertrand Lembège, J. Stienlet

JOURNAL OF GEOPHYSICAL RESEARCH: SPACE PHYSICS, VOL. 118, 1132–1145, doi:10.1002/jgra.50158, 2013

On the origin of the quasi-perpendicular ion foreshock: Full-particle simulations

P. Savoini,[1] B. Lembege,[2] and J. Stienlet[1]

Received 14 June 2012; revised 21 January 2013; accepted 27 January 2013; published 25 March 2013.

[1] Many space missions have already evidenced the existence of the ion foreshock region located upstream of the Earth's bow shock and populated by energetic backstreaming ions reflected by the shock front. In order to analyze this region, a curved shock is simulated with a 2-D particle-in-cell (PIC) code. The analysis is presently restricted to the quasi-perpendicular angular range defined by $45° \leq \theta_{Bn} \leq 90°$. In agreement with experimental data, present results evidence two distinct ion populations backstreaming from the shock front along the interplanetary magnetic field: (i) the *field-aligned beam* population (hereafter "FAB") and (ii) the *gyrophase bunched* population (hereafter "GPB") which differ from each other by their gyrotropic or non-gyrotropic behavior, respectively. Excluded by a simulation time which is too short, ion instabilities pitch-angle scattering cannot be the source of "GPB." Two new criteria are proposed to identify more precisely each population: their interaction time Δt_{int} with the shock front and their downstream penetration depth. These criteria show that (i) the "FAB" population moves back and forth between the upstream edge of the shock front and the overshoot, and is characterized by a Δt_{int} covering several upstream gyroperiods. (ii) In contrast, the "GPB" ions suffer a short interaction time (i.e., $1 < \tau_{ci}$). We observe that the "FAB" ions may have different origins although all "GPB" ions seem to be produced by the electrostatic field built up at the shock and are emitted in a burst-like mode rather than in continuous way.

Citation: Savoini, P., B. Lembege, and J. Stienlet (2013), On the origin of the quasi-perpendicular Ion Foreshock: Full-particle simulations, *J. Geophys. Res. Space Physics.*, *118*, 1132–1145, doi:10.1002/jgra.50158.

1. Introduction

[2] Collisionless shocks are common structures in space and astrophysical environments which dissipate bulk flow kinetic energy and can accelerate a large fraction of particles. Spacecraft have firmly established the existence of the so-called foreshock region magnetically connected to the shock and filled with energized particles backstreaming from the shock front [*Tsurutani and Rodriguez*, 1981; *Paschmann et al*., 1981; *Bonifazi and Moreno*, 1981a, 1981b; *Fuselier*, 1995; *Eastwood et al*., 2005; *Oka et al*., 2005; *Kucharek*, 2008]. This region is populated both by energetic electrons and ions and is associated with wave activity [*Shin et al*., 2008; *Přech et al*., 2005; *Mazelle et al*., 2003; *Kuncic et al*., 2004; *Kis et al*., 2007; *Hoshino and Terasawa*, 1985; *Constantinescu et al*., 2007].

[3] The energization of these species depends roughly on two parameters: the angle θ_{Bn} defined between the normal to the shock front and the upstream magnetic field, and the Mach number M_A. As consequence, accelerated electron and ion sources are distributed differently over the bow shock curvature and allow to distinguish spatial regions within the overall foreshock dominated by different species and energies (see *Eastwood et al.* [2005] for a review).

[4] In the present study, we will only focus on the reflected ions where five different ion groups can be identified based on their velocity space signature [*Bonifazi and Moreno*, 1981a, 1981b; *Fuselier*, 1995; *Oka et al*., 2005]: (i) a noticeable percentage of ions is reflected by the electrostatic potential jump at the shock ramp as observed for supercritical shock (so-called "gyrating ions" in the literature); these ions are responsible for the formation of the foot and are not strictly a part of the ion foreshock since they are transmitted downstream after one gyration; (ii) the field-aligned beam (FAB) ions moving along the foreshock boundary [*Thomsen et al.*, 1983a; *Schwartz and Burgess*, 1984; *Oka et al.*, 2005; *Meziane et al.*, 2005; *Mazelle et al.*, 2005]; (iii) the gyrophase bunched (GPB) ions grouped into packets with the same gyrophase [*Gurgiolo et al.*, 1983]; (iv) the diffuse ions characterized by a very broad flat energy spectra (extending up to 100*kev*) and produced

[1]LPP-Ecole polytechnique-UPMC, Laboratoire de Physique des Plasmas, Ecole polytechnique, Palaiseau, France.
[2]LATMOS-UVSQ-IPSL-CNRS, Guyancourt, France.

Corresponding author: P. Savoini, LPP-Ecole polytechnique-UPMC, Laboratoire de Physique des Plasmas, Ecole polytechnique, Route de Saclay, 91128 Palaiseau Cedex, France. (Philippe.savoini@upmc.fr)

2169-9380/13/10.1002/jgra.50158

upstream of a quasi-parallel region ($0° \leq \theta_{Bn} \leq 45°$) [*Winske and Leroy*, 1984; *Kucharek and Scholer*, 1991; *Kis et al*., 2004; *Bonifazi and Moreno*, 1981a, 1981b; *Gosling et al*., 1982]; and (v) the intermediate ions which are a combination of (ii) and (iv) populations [*Oka et al.*, 2005]. Among these five groups, only the origin of the gyrating ions has been identified, while the formation mechanism of the other ion groups has not been clearly established yet. Nevertheless, experimental data have evidenced that the high energy ion beams (FAB) (tens of *keV*) [*Kucharek et al.*, 2004; *Meziane et al.*, 2005] are observed near the upstream edge of the ion foreshock. However, as the magnetic field lines are convected further downstream within the ion foreshock, the backstreaming ions are successively characterized by a gyrophase bunched population, by an intermediate-type population, and finally by the diffuse type population. Then the first three distribution types (i)–(iii) can be associated to the quasi-perpendicular region of the bow shock (i.e., where $45° \leq \theta_{Bn} \leq 90°$), while the two last populations (iv)–(v) are more associated to the quasi-parallel region (i.e., when $0° \leq \theta_{Bn} \leq 45°$) with an intermediate population lying at the transition between the quasi-parallel and quasi-perpendicular regions.

[5] Even if the generation and the acceleration mechanism of these different ion groups have received a lot of attention within the past few decades, these are not fully understood yet. The difficulty is that the study of the origin of these populations needs to include both the micro-scale of the shock wave (including the kinetic effects of the different populations) and the macro-scale associated to the curvature of the shock front which is an essential component in the generation of the foreshock region. Then only numerical simulations of curved shock wave allow to investigate all these scales simultaneously as was done with hybrid simulations (kinetic ions, fluid electrons) [*Thomas and Winske*, 1990; *Omidi et al.*, 2005, 2006; *Blanco-Cano et al.*, 2006a, 2006b; *Sibeck et al.*, 2008; *Blanco-Cano et al.*, 2009] for the ion foreshock and more recently by 2-D full-particle simulations for the electron foreshock [*Savoini and Lembège*, 1999, 2001]. To our knowledge, it was the first time that full-particle simulations have been performed including self-consistently the curvature of a supercritical shock wave and the time-of-flight effects. Although these 2-D PIC simulations have been limited to the quasi-perpendicular angular domain, these have allowed to identify the different origins of the backstreaming electrons. The present paper generalizes this approach and extends it to the ion foreshock but is limited intentionally to the quasi-perpendicular angular domain. As a consequence, we will focus only on the first three ion populations, i.e., the gyrating ions, the "FAB", and the "GPB" populations.

[6] *Meziane et al.* [2005] has recently reviewed the FAB properties which are composed with collimated ion beams with an energy of a few *keV* (typically $\approx 15keV$) that propagate away from the shock [*Paschmann et al.*, 1980; *Thomsen et al.*, 1983b; *Meziane et al.*, 2004a]. In short, the FAB ions are observed in the quasi-perpendicular domain between $40° \leq \theta_{Bn} \leq 75°$ [*Bonifazi and Moreno*, 1981a; *Paschmann et al.*, 1980; *Meziane*, 2005] with a density decreasing as θ_{Bn} increases. Obviously, backstreaming ion beams are considered the most important source of free energy in the foreshock region. As discussed by *Gary et al.* [1981], the electromagnetic ion-ion cyclotron instability is a good candidate to heat the FAB particularly along the parallel direction and can be observed in association with gyrating ion distribution [*Meziane et al.*, 2001; *Mazelle et al.*, 2003]. Nevertheless, such a behavior seems in contradiction to the observation of the FAB ions which persist far upstream from the terrestrial bow shock (over $\approx 93R_E$) when the thermalization is supposed to have already taken place. The last important properties of these FAB is the temperature anisotropy $T_\perp/T_\parallel$ observed in the range 4–9 [*Paschmann et al.*, 1981] with a magnitude of $T_\perp$ much larger than the solar wind perpendicular temperature (by a factor $\approx$ 20–200). Concerning the origin of the FAB, different "scenarii" have been elaborated [*Möbius et al.*, 2001; *Kucharek et al.*, 2004], all of them having some drawbacks: (i) the models based on the guiding center approximation (specular reflection) [*Sonnerup*, 1969; *Paschmann et al.*, 1980; *Schwartz et al.*, 1983; *Schwartz and Burgess*, 1984; *Gosling et al.*, 1982] with or without the conservation of the magnetic moment, (ii) the leakage of some magnetosheath ions which can produce low energy FAB [*Edmiston et al.*, 1982; *Tanaka et al.*, 1983; *Thomsen et al.*, 1983a], (iii) the diffusion of some reflected ions ("gyrating ions") by upstream magnetic fluctuations [*Giacalone et al.*, 1994], or (iv) the ion diffusion which takes place directly in the shock ramp (pitch angle scattering during the reflection process) [*Kucharek et al.*, 2004; *Bale et al.*, 2005].

[7] The "GPB" ions characterized by their non-gyrotropic nature are found at some distance from the shock front [*Thomsen et al.*, 1985; *Fuselier et al.*, 1986a]. To build up and to sustain a non-gyrotropic distribution, it is necessary to synchronize the gyrophase angles of the particles by some process. This synchronization may be due to mechanisms which are phase dependent in velocity space as trapping by low-frequency monochromatic waves [*Mazelle et al.*, 2003; *Hamza et al.*, 2006], as burst-like mode of reflection inducing temporal modulation of the ion distribution [*Gurgiolo et al.*, 1983; *Motschmann et al.*, 1999] or as beam-plasma instabilities [*Hoshino and Terasawa*, 1985] which trap ions and can cause the gyrophase bunched distribution. However, it is quite difficult to discriminate between these different possibilities which can be present separately in time or simultaneously.

[8] Herein, we will take advantage of the simulation of the whole quasi-perpendicular angular domain in a self-consistently way to investigate the problem of the origin of the reflected ion populations on the basis of a statistical analysis of the particle trajectories. The plan of the paper is as follows. In section 2, we briefly describe the numerical simulations performed for analyzing a curved supercritical shock and its associated ion foreshock. In section 3, we present the different ion populations identified versus the distance from the shock front and the angular range of the curved front, and the criteria commonly used to discriminate between them. The necessity for new selection criteria will be presented and detailed in section 4, while conclusions on the most plausible origins of the different ions populating the quasi-perpendicular ion foreshock will be drawn in section 5.

2. Description of the Numerical Simulations

[9] The present simulations have been performed with a 2 – 1/2 dimensional, fully electromagnetic, relativistic particle code using standard finite-size particle techniques. Details have been already given in *Lembege and Dawson* [1987] for 1-D and in *Lembege and Savoini* [1992] for 2-D simulations of planar shocks. Simulations have been extended to 2-D curved shock [*Savoini and Lembège*, 2001; *Savoini et al.*, 2010]. Basic properties of the numerical code can be summarized as follows. The simulation box is divided into two parts, vacuum and plasma. Fields are separated in electromagnetic transverse components, hereafter denoted by a subscript "*t*," and the electrostatic longitudinal components, hereafter denoted by a subscript "*l*," which results from the space-charge effects. Non-periodic conditions are applied along *x*-direction within the simulation box, and periodic conditions are used along *y*-direction. Lengths of the plasma simulation box are $\widetilde{L}_x = 6144$ and $\widetilde{L}_y = 8192$, which represent 205 and 274 ion inertial lengths $\left(\widetilde{c}/\widetilde{\omega}_{pi}\right)$, respectively. All normalized quantities are indicated with a tilde "~".

[10] The shock is created with a cylindrical magnetic piston generated by applying an external current pulse. The curvature of the shock front is determined by the geometry of the applied current. One important point concerns the orientation of the magnetostatic field $\vec{B}_o$ which is partially lying outside the simulation plane as in *Savoini and Lembège* [2001]. The curvature (roughly half circle) of the generated shock front allows herein a continuous variation of θ_{Bn} from 90° to 45° simulating the whole quasi-perpendicular domain of shock propagation. The radius of the magnetic cylinder (used as a magnetic piston) has been chosen carefully so that after a short transient period $\widetilde{t} \leq 0.3\widetilde{\tau}_{ci}$, the curvature radius $\widetilde{R}_c$ of the shock is much larger than the upstream ion Larmor gyroradius $\widetilde{\rho}_{ci}$ $\left(\widetilde{R}_c \geq 20\widetilde{\rho}_{ci}\right)$, where $\widetilde{\tau}_{ci}$ is the upstream ion gyroperiod. At the end of the simulation, this radius is about $\widetilde{R}_c \approx 140\widetilde{\rho}_{ci}$.

[11] Sizes of the simulation box and time of the run are large enough to cover all characteristic space and timescales for both particle species $\left(\widetilde{t}_{\text{simul}} = 5.4\widetilde{\tau}_{ci}\right)$ and so we observe the first stage of the formation of the ion foreshock. These values are large enough to investigate the backstreaming ions after they interact with the shock front. Initial plasma conditions are summarized as follows: light velocity $\widetilde{c} = 3$ and temperature ratio between ion and electron population $T_e/T_i = 1.58$. A mass ratio $m_i/m_e = 84$ is used in order to save CPU time, and the Alfvèn velocity is $\widetilde{v}_A = 0.16$. The shock is in supercritical regime with an Alfvèn Mach number $M_A = \widetilde{v}_{\text{shock}}/\widetilde{v}_A \approx 3.8$ measured at $\theta_{Bn} = 90°$ (which is used as a reference angle). The main upstream plasma parameters values are summarized in Table 1 for both electrons and ions.

Table 1. Upstream Numerical Parameters

Parameters	Electrons	Ions
$\widetilde{v}_{th}$	0.3	0.026
$\widetilde{\lambda}_D$	0.42	0.33
$\widetilde{\rho}_c$	0.84	56
$\widetilde{c}/\widetilde{\omega}_p$	3	30
$\widetilde{\omega}_c$	0.5	0.006
$\widetilde{\omega}_p$	1	0.1
$\widetilde{\tau}_c$	13	1047
$\widetilde{\beta}$	0.16	0.10
$\widetilde{V}_A$	0.23	0.23

3. The Foreshock Results

[12] To the knowledge of the authors, this work presents the first 2-D PIC simulations of the ion foreshock in the presence of a self-consistent curved shock. Previous simulations of shocks including curvature effects [*Thomas and Winske*, 1990; *Omidi et al.*, 2005, 2006; *Blanco-Cano et al.*, 2006a, 2006b; *Sibeck et al.*, 2008; *Blanco-Cano et al.*, 2009] used hybrid codes which treated electrons as a massless fluid; more importantly, in such simulations, the intrinsic non-stationary behavior of the shock front was excluded. In particular, one invoked source of non-stationary is based on the self-reformation of the shock front due to the accumulation of reflected ions as observed in 1-D [*Lembege and Dawson*, 1987; *Hada et al.*, 2003; *Yang et al.*, 2009] and 2-D PIC simulations [*Lembege and Savoini*, 1992], or on the thermalization of reflected ions taking place within the foot region under two-stream instability [*Matsukiyo and Scholer*, 2006; *Scholer and Matsukiyo*, 2004]. Indeed, the evidence of the self-reformation in hybrid simulations requires a spatial resolution high enough as described in *Hellinger et al.* [2002] and was not reported in the previous papers dedicated to curved shock simulations. Moreover, the non-stationarity of the terrestrial shock front has been clearly evidenced also in CLUSTER-II experimental data [*Horbury et al.*, 2001; *Lefebvre et al.*, 2010; *Mazelle et al.*, 2010].

[13] More important, it is worth pointing out that the "time-of-flight" effect is fully included in the present simulation. As a result, backstreaming particles (electrons and ions) collected further from the shock correspond to particles having interacted with different parts of the curved shock front (i.e., different θ_{Bn} angles) depending on their local respective parallel velocity value. Fast particles collected from an observer are related to the magnetic field line connecting directly the nearest point of the curved shock to the observer location, while slower particles come from other parts. In the solar wind frame (i.e., frame of the present simulation), an equivalent situation is obtained as a given magnetic field line connected from the expanding curved shock will "scan" different angles θ_{Bn} in time [*Savoini and Lembège*, 2001]. Nevertheless, the present paper is focused only on the ion foreshock.

3.1. Main Features of the Ion Foreshock

[14] Figure 1a shows the amplitude of the main magnetic field component at the curved shock front at the end of the simulation $\left(\widetilde{T}_{\text{sim}} \approx 5.4\widetilde{\tau}_{ci}\right)$ and the associated ion foreshock upstream. The enlarged view of the more oblique part of the curved shock (Figure 1b) shows (i) a well-developed electromagnetic precursor which propagates ahead from the shock front within the angular range $45° \leq \theta_{Bn} \leq 55°$, and (ii) the presence of small wave activity both on electromagnetic $\left(\delta\widetilde{B}/\widetilde{B} \approx 0.02\right)$ and electrostatic field components, which is correlated with the electron foreshock (see the red arrow in Figure 1a). These later fluctuations are too

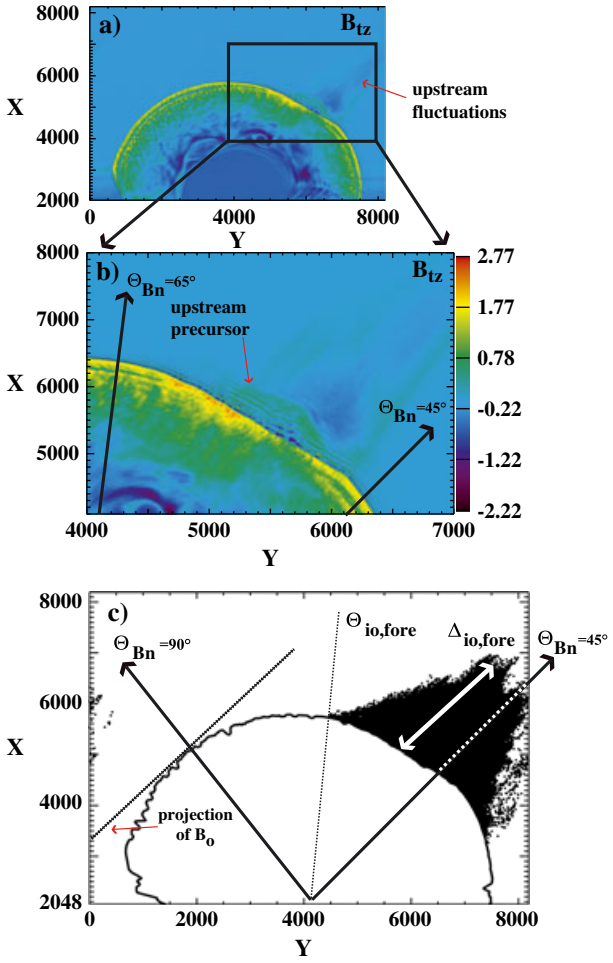

Figure 1. View of the developed curved shock within the simulation plane $X-Y$ plotted at time $\widetilde{t} = 5.4\widetilde{\tau}_{ci}$ where $\widetilde{\tau}_{ci}$ is the upstream cyclotron ion period. (a) shows the main magnetic field component $\widetilde{B}_{tz}$. The ambient magnetostatic field $\widetilde{B}_o$ (representing the interplanetary magnetic field) is imposed along a direction of 45° outside the simulation plane. Then the whole angular range of curved shock is lying within $45° \leq \theta_{Bn} \leq 90°$. (b) is an enlarged view of the $45° \leq \theta_{Bn} \leq 65°$ region showing details of the upstream magnetic field. (c) plots the ions locations within the ion foreshock where backstreaming ions satisfied the criteria detailed in the text. For reference, straight arrows represent the normal of the shock front at $\theta_{Bn} = 90°$ and $\theta_{Bn} = 45°$. The dotted line represents the projection of the upstream field $\widetilde{B}_o$ into the simulation plane. Two parameters have been also reported: (i) $\theta_{\mathrm{io,fore}}$ ($\approx 66°$) the leading edge angle of the ions foreshock and (ii) $\Delta_{\mathrm{io,fore}}$ the extend of the ion foreshock measured from the curved front at the end of our simulation.

small to have an impact on the upstream ions. On the other hand, the ion foreshock is presently analyzed within a time range too short to allow the triggering of any ion instability excited by the backstreaming ions within the foreshock region $\left(\widetilde{T}_{\mathrm{instability}}/\widetilde{T}_{\mathrm{run}} \approx 1.1\right)$ [*Gary*, 1981]. As a consequence, the ion foreshock can be considered here as free of instabilities which could have some impact on the ion population.

[15] Reflected/backstreaming ions need to satisfy two criteria to be selected : (i) ions have to be in the upstream region at the end of the run, and (ii) these must have interacted with the shock front during the run time interval. These criteria allow us to identify two distinct ion populations. The *reflected (so-called "gyrating") ions*, observed just upstream of the shock front but which are not a part of the ion foreshock and the *backstreaming ions* which contribute to this particular region. Then in a second step, we refine this selection by keeping only the backstreaming ions as plotted in Figure 1c. In agreement with an estimate deduced from experimental measurements [*Kucharek et al.*, 2004], we found that the ion foreshock is composed of about 2% of the total incoming solar wind which has interacted with the bow shock.

[16] As evidenced in Figure 1c, backstreaming ions are not uniformally distributed within the whole foreshock. Then one can define a critical angle, defining the upstream edge of the ion foreshock around $\theta_{\mathrm{io,fore}} \approx 66°$ with respect to the upstream $\widetilde{B}_o$ field. In addition, ions are not uniformly distributed around $\theta_{Bn} = 45°$ but form a strip slightly above this angle. Presently, its maximal upstream spatial extension (limited by the simulation time) covers about a distance $\Delta_{\mathrm{io,fore}} \approx 130\widetilde{c}/\widetilde{\omega}_{pi}$.

3.2. Backstreaming Ion Distribution Function

[17] In order to analyze in detail the dynamics of the backstreaming ions in a second step, we have mapped the whole ion foreshock region into 20 sampling boxes within which local ion distribution functions are computed. The size of each sampling box has been chosen so that it is small enough to follow the progressive changes in local distributions (versus both the local direction θ_{Bn} and the distance with respect to the shock front) but large enough to satisfy some reasonable statistics. Shape and locations of sampling boxes are aligned along the magnetic field lines projected within the simulation plane. This procedure allows to keep roughly the same size for all sampling boxes in order to reproduce a constant sampling rate. Reporting results for all boxes can be misleading. Instead, we have only reported in Figure 2 typical local velocity distribution found within three selected sampling boxes. For each selected box, $\widetilde{v}_{\parallel}$ versus $\widetilde{v}_{\perp 1}$ and $\widetilde{v}_{\perp 1}$ versus $\widetilde{v}_{\perp 2}$ distributions are plotted, respectively, in the upper and lower parts of this figure; parallel and perpendicular directions are defined with respect to the local $\widetilde{B}$ field. The locations of the three selected boxes (Figure 2d) correspond to a progressive deviation from $\theta_{Bn} = 90°$ when staying along the shock front (Figures 2a and 2b), and to an increasing distance from the shock front into the ion foreshock (Figures 2b and 2c). Obviously, plots are more noisy along the upstream edge of the foreshock (Figure 2a) and far from the shock front (Figure 2c), since the local number of selected ions is low. All backstreaming ions do have a finite parallel velocity (top panels of Figure 2) but differ by their characteristic perpendicular distributions (bottom panels). Different behavior can be identified as follows:

[18] 1. In Figure 2a defined for $59° \leq \theta_{Bn} < 66°$, the backstreaming ions (hereafter named population 1) form a gyrotropic distribution characterized by a clear ring in the perpendicular distribution $(\widetilde{v}_{\perp 1}, \widetilde{v}_{\perp 2})$ indicating that parti-

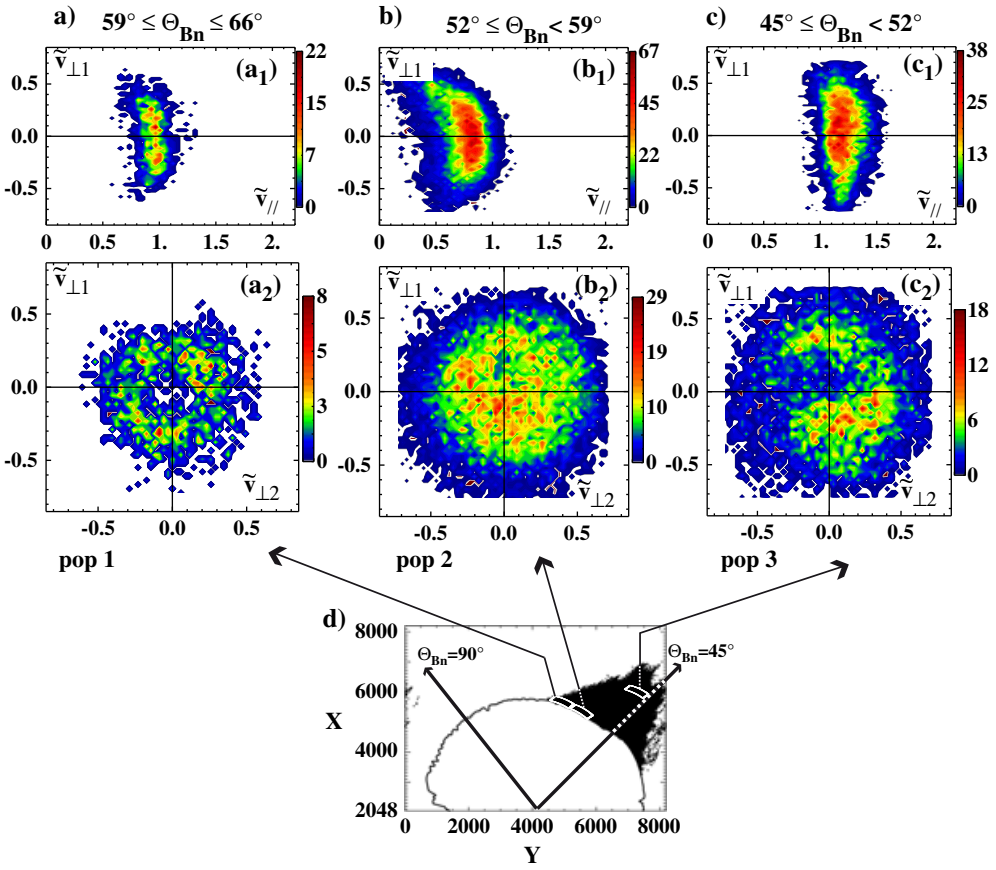

Figure 2. Local ion velocity distribution measured in the foreshock region (only backstreaming ions are selected; the solar wind is excluded). The two different planes $(\widetilde{v}_{\parallel}, \widetilde{v}_{\perp 1})$ and $(\widetilde{v}_{\perp 1}, \widetilde{v}_{\perp 2})$ are plotted in top and lower panels, respectively. Velocity distribution functions are measured (i) near the edge of ion foreshock for $59° \leq \theta_{Bn} < 66°$ ("pop 1" of (a)), (ii) near the shock front but for lower θ_{Bn} angular range, $52° \leq \theta_{Bn} < 59°$ ("pop 2" of (b)), and finally (iii) much deeper in the foreshock far from the shock front for $45° \leq \theta_{Bn} < 52°$ ("pop 3" of (c)). For reference, (d) shows the locations of the sampling boxes where velocity distributions of populations 1 (pop 1), 2 (pop2), and 3 (pop3) are measured within the ion foreshock, respectively.

cles gyrophase together and therefore arrive from all directions perpendicular to the magnetic field. Then the incoming ions with a small perpendicular velocity (no particle appears in the $|\widetilde{v}_{\mathrm{perp}}| \leq 0.2$ domain) are entirely transmitted into the downstream region and do not participate to the final ion foreshock. In the present results, ions directly reflected by the shock front (so-called "gyrating" ions) are near the shock front. These have been removed from the statistics of ions which participate to the ion foreshock and are excluded in plots of Figure 2. One important point is the presence of backstreaming particles at the upstream edge of the ion foreshock, corresponding to ions newly reflected back by the shock front. Indeed, these particles have not suffered any time-of-flight effect and are produced by the interaction with the local shock front ("local" means the part of the shock front nearest to the observer). Resulting backstreaming population can be also observed in CLUSTER experimental data [see, for example, *Meziane et al.* [2007], Figure 3]. In the present case, the reflected ions do have a mean parallel bulk velocity around $\widetilde{v}_{\parallel} \approx 0.95$ which is higher than the parallel shock front velocity $(\widetilde{v}_{\mathrm{shock},\parallel} \approx 0.6)$.

[19] The ion foreshock has a finite extension in angular range as shown in Figure 1c. One can determine a theoretical angle $\theta_{\mathrm{io,\,th}}$ where reflected ions succeed to escape into the upstream region. Indeed, their parallel guiding-center velocity $\widetilde{v}_{gc\parallel i}$ has to be larger than the parallel shock wave velocity. As consequence, a simple relationship can be defined between this angle and the shock velocity given by:

$$\theta_{\mathrm{io,\,th}} \leq cos^{-1}\left(\frac{M_A v_A}{\widetilde{v}_{gc\parallel i}}\right)$$

Then we obtain a theoretical value $\theta_{\mathrm{io,\,th}} \approx 65°$ which is in good agreement with the angular extension of the ion foreshock defined by the angle $\theta_{\mathrm{io,\,fore}} \approx 66°$ measured directly from Figure 1 (section 3.1).

[20] 2. In Figure 2b defined for $52° \leq \theta_{Bn} < 59°$, we find a distribution approximately gyrotropic (hereafter named population 2) in the $(\widetilde{v}_{\perp 1}, \widetilde{v}_{\perp 2})$ space. Obviously,

as θ_{Bn} decreases, the criterion $\widetilde{v}_{gc\|i} \geq \widetilde{v}_{\text{shock}\|}$ is less restrictive and the average parallel velocity $\widetilde{v}_{gc\|i}$ decreases from 0.95 to 0.8 between Figures 2a and 2b. As for Figure 2a, the distribution in $(\widetilde{v}_{\perp 1}, \widetilde{v}_{\perp 2})$ space can be considered as gyrotropic, even if the part $\widetilde{v}_{\perp 2} < 0$ looks more asymmetric as compared with the part $\widetilde{v}_{\perp 2} > 0$. Herein, the local velocity distribution includes ions which are newly reflected and are then directly accelerated at the shock front. Then these reflected ions suffer two distinct acceleration processes characteristic of an oblique shock in a quasi-perpendicular range: (i) a parallel acceleration by the parallel macroscopic electrostatic component $\widetilde{E}_{l\|}$ at the front and (ii) a perpendicular acceleration (by the $\widetilde{E}_{l\perp} \times \widetilde{B}$ drift) before escaping into the upstream region.

[21] 3. Finally, Figure 2c defined for $45° \leq \theta_{Bn} < 52°$ presents an ion population (hereafter named population 3) measured far away from the shock front (and at less oblique shocks). Note that this local distribution function measured at a certain distance from the shock front illustrates quite well the backstreaming ions suffering the "time-of-flight" effects. Indeed, Figures 2a and 2b correspond to particles having freshly interacted with the shock front. In contrast with Figure $2b_2$, Figure $2c_2$ shows a non-gyrotropic population. Differences also appear in the parallel direction, where the ions parallel bulk velocity increases from $\widetilde{v}_{\|} \approx 0.8$ near the shock front (Figure $2b_1$) to $\widetilde{v}_{\|} \approx 1.2$ (Figure $2c_1$), further from the shock front. Indeed, the distance from the shock front plays the role of a filter, and only the most energetic ions can be observed at large distances from the shock front.

[22] Then Figure 2 illustrates the three different characteristic distributions observed in our simulation. Furthermore, the measurements of the local velocity distributions in the other sampling boxes (not shown here) confirm that the gyrotropic populations (named "FAB") appear near the shock front at any angle ($45° \leq \theta_{Bn} \leq 90°$) and populates the edge of the ion foreshock at any distance from the shock front. However, more deeply into the foreshock, this population is replaced by a gyrophase bunch population (named "GPB") characterized in $(\widetilde{v}_{\perp 1}, \widetilde{v}_{\perp 2})$ space by a rotation in the clockwise direction around the upstream magnetic field B_o as observed experimentally by [*Mazelle et al.*, 2005]. Along the shock front, we observe an increase of the parallel bulk velocity as θ_{Bn} decreases from 66° to 45° (the distribution defined near the shock front around $\theta_{Bn} = 45°$ is not shown). This increase is mainly due to a filtering effect where only ions with the projected parallel velocity (in the simulation plane) larger than the shock front velocity succeed to escape into the upstream region. Moreover, we measure a local temperature anisotropy within the different sampling boxes around $T_{\perp}/T_{\|} \approx 3$ which is also in good agreement with the experimental data *Fuselier et al.*, 1986a; *Meziane*, 2005. Present results confirm that this temperature anisotropy does not change during the whole simulation time and over long distances from the shock front.

3.3. The "FAB" and "GPB" Populations

[23] Simulation results of Figure 2 recover the two typical ion foreshock populations observed experimentally in the quasi-perpendicular domain of propagation. Both consist of ions collimated along the interplanetary magnetic field (IMF). In order to separate more clearly the two populations, we can make use of the pitch angle α parameter in addition to the gyrotropic or the non-gyrotropic signature of these two populations. Indeed, experimental observations evidence that the "FAB" population has a pitch angle $0° \leq \alpha \leq 20°$ [*Fuselier et al.*, 1986a; *Eastwood et al.*, 2005] smaller than for the "GPB" population $20° \leq \alpha \leq 90°$ [*Meziane et al.*, 2007]. Nevertheless, such a distinction from particle observations alone is usually quite arbitrary. In practice, the two populations seem more easily discriminated by analyzing their possible association with wave activity. More precisely, "GPB" populations are observed in association with large-amplitude ($\Delta B/B \approx 1$) and weakly compressive ULF waves [*Fuselier et al.*, 1986b], whereas these ULF waves are always absent when the "FAB" populations are observed [*Hoppe et al.*, 1982; *Meziane et al.*, 2001; *Mazelle et al.*, 2003]. A strong wave activity is in favor of an important pitch angle scattering which is expected to lead to a destruction of any coherent structure in the local distribution as observed in GPB. In contrast, a weak wave activity will be rather associated to a weaker pitch angle scattering as observed in FAB. In the present simulations, such wave activity in low-frequency range is naturally excluded because of the short duration of the present simulations (section 3.1), and new criteria have to be defined in order to differentiate the two populations as detailed in section 4.

[24] In fact, more important than the α values range mentioned above, the shape of the pitch angle distribution can provide information on the nature of the backstreaming ions. This will allow us to analyze whether these distributions can persist without invoking any possible wave activity. Figure 3 represents sketches of two pitch angle configurations commonly used for identifying both populations. The "FAB" population (Figure 3a) is characterized by a maximum at $\alpha \approx 0°$ which decreases rapidly as α increases, although the "GPB" population (Figure 3b) exhibits a maximum for higher pitch angle, usually around $\alpha \approx 20°$–$40°$ and, more important, no particle at $\alpha \approx 0°$. Then in order to establish a link with experimental observations, we will define as "FAB" the ions exhibiting a gyrotropic distribution in the perpendicular velocity plane and a pitch angle with a maximum for $\alpha \approx 0°$, and as "GPB" the ions exhibiting a gyrophase bunch distribution and a finite pitch angle value different from 0°.

[25] Figure 4 shows pitch angle particles distribution corresponding to the populations identified in Figure 2 and leads to the following statements:

[26] 1. First, the population 1 of Figure 2a observed near the shock front at the edge of the ion foreshock cannot be rigourously considered as a "FAB" population since the pitch angle distribution presents a maximum around a finite angle value, $\alpha \approx 17°$ (Figure 4a). Nevertheless, it cannot be considered strictly as a "GPB" population neither because of their gyrotropic distribution around the magnetic field (Figure 2a). As already emphasized, this population has just been reflected back by the shock front, and no gyrophase mixing is expected [*Gurgiolo et al.*, 1983]. Then one considers the gyrotropic criterion as the dominant feature, and one may classify this

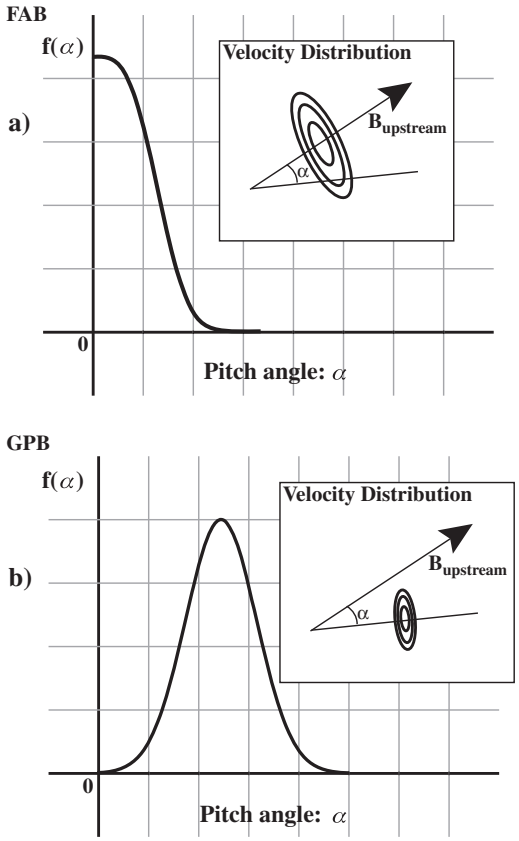

Figure 3. Schematic plots of "FAB" (a) and "GPB" (b) pitch angle ion distributions $f(\alpha)$ deduced from the observations within the quasi-perpendicular foreshock region.

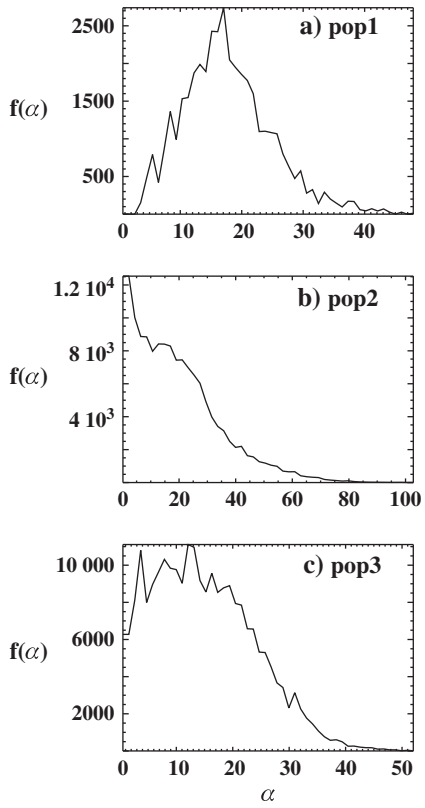

Figure 4. Pitch angle distributions $f(\alpha)$ of populations 1, 2, and 3, measured respectively, within the three sampling boxes of Figure 2, when the pitch angle α is defined by $\vec{v} \cdot \vec{B} = vB\cos(\alpha)$.

kind of distribution as "FAB" population [*Meziane et al.*, 2007].

[27] 2. Second, in a first approach, the population 2 of Figure 2b cannot be classified since it seems to include two distribution components: a low-pitch angle component defined for $\alpha < 10°$ (as could be classified as "FAB") and a high-pitch angle component centered around a finite value $\alpha \approx 15°$–$20°$ (as could be classified as "GPB"). As shown in next section 4, this distribution will be explained in terms of populations mixing.

[28] 3. Third, the same problem appears also for the population 3 where the pitch angle distribution of Figure 4c seems in agreement with a "GPB" population (as classified in Figure 3a) with a maximum around $\alpha \approx 10°$–$15°$ and a perpendicular velocity (Figure 2c) which evidences roughly a gyrophase bunched distribution. Nevertheless, the pitch angle does not go down to 0° (as one could expect) which is clearly a "FAB" signature mixing with a "GPB" population.

[29] Obviously, with the above definitions commonly used, the discrimination between the different populations is not precise at all, and the results of Figures 4a–4c are more complicated to analyze than expected. One possibility to explain this difficulty is that both populations are mixed together in the velocity space, and this mixing is more or less reinforced according to the location of the sampling box (versus angle and distance from the shock front). For clarifying this point, we have defined new additional criteria able to discriminate the "FAB" and the "GPB" populations which must be independent on the perpendicular and parallel velocity component (i.e., no relationship with our criteria used previously). As explained in section 4, our new criteria will provide some clues for understanding the source and the acceleration mechanisms involved not only in the foreshock formation but also in determining its morphology.

4. Discussion

[30] At this stage, we will use the limitation of the present PIC simulations to our advantage. Effectively, as already pointed out, the simulation time is not long enough to allow ion instabilities to develop [*Gary*, 1981]. Then in the absence of instabilities, our results do not support the origin of the "GPB" population as produced by large-amplitude waves which trap ions and cause the phase bunching of the distribution via a so-called beam disruption mechanism [*Hoshino and Terasawa*, 1985; *Mazelle et al.*, 2003; *Meziane et al.*, 2004b]. With this limitation in mind, the evidence of "FAB" and "GPB" populations within the foreshock (as defined in the Figures 2b and 2c) leads to the conclusion that both populations are generated by the shock front itself in our simulation. Such situation is seldom but has been already mentioned in the Earth's foreshock.

For example, *Meziane et al.* [2004a] observes one event with gyrophased bunched ions produced by specular reflection for $\theta_{Bn} \approx 40°$, while *Kucharek et al.* [2004] analyzes the production of "FAB" population by the shock front for $\theta_{Bn} \approx 70°$.

[31] With this approach, we have searched new criteria which have to be relevant whatever the reflection mechanism is. Figures 5a–5c plot the ions interaction time range $\Delta\widetilde{t}_{int}$ versus their depth of penetration into the shock front (herein $\widetilde{L}_{depth}$) for the three selected boxes of Figure 2. This interaction time range is defined by $\Delta\widetilde{t}_{int} = \widetilde{T}_{out} - \widetilde{T}_{in}$ where $\widetilde{T}_{in}$ is the time when the particle is entering into the shock front and $\widetilde{T}_{out}$ is the time at which particles leave the shock front and re-enter definitively into the upstream region. The word "definitively" is important since ions can go back and

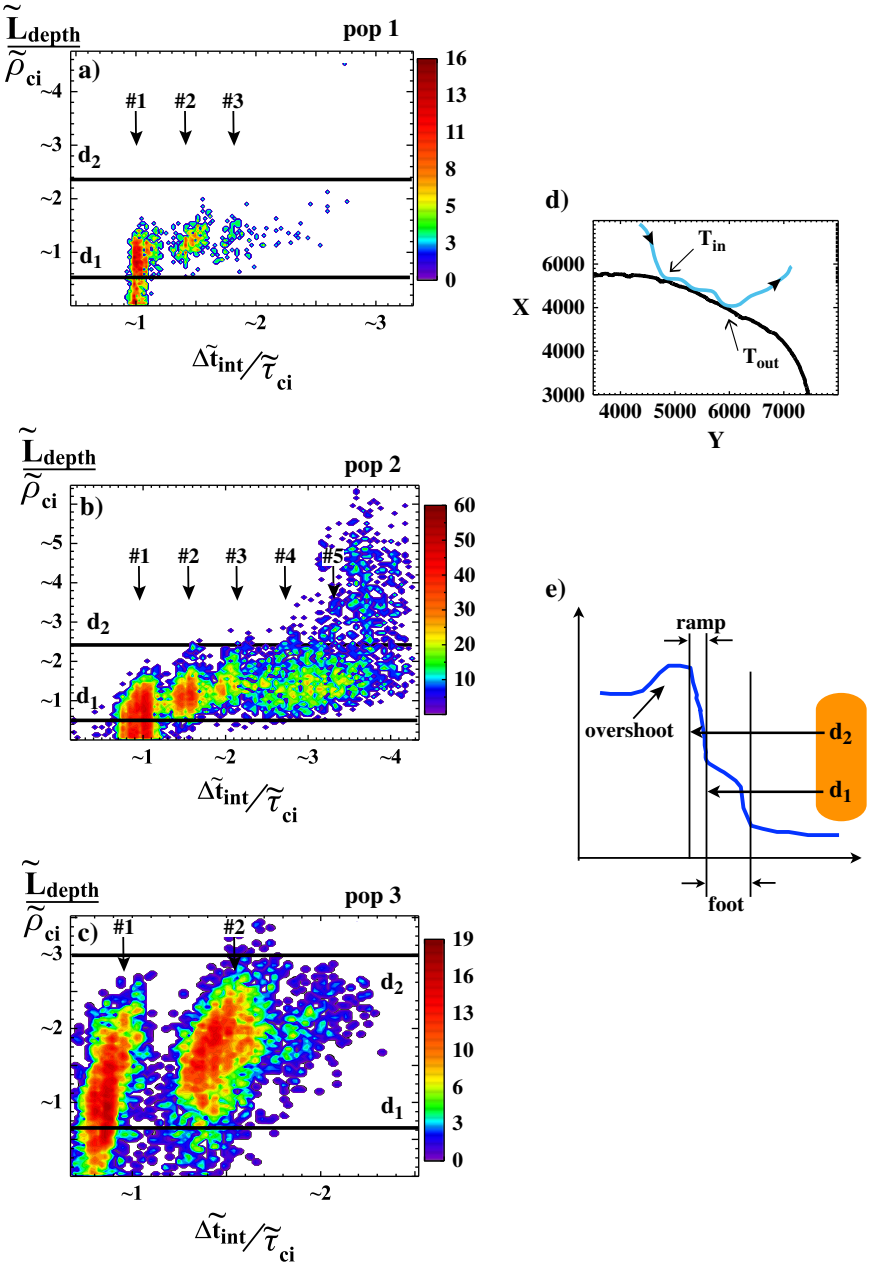

Figure 5. (a–c) show the penetration depth $\widetilde{L}_{depth}$ of incoming ions through the shock front (normalized to the upstream ion gyroradius $\widetilde{\rho}_{ci}$) before being reflected back upstream versus the total interaction time $\Delta\widetilde{t}_{int}$ with the shock front (normalized to the upstream ion gyroperiod $\widetilde{\tau}_{ci}$) for each population 1, 2, and 3 defined in Figure 2, respectively. On each plot, the different "burst" have been labeled #1, #2, ... The interaction time $\Delta\widetilde{t}_{int}$ is illustrated in (d) where $\Delta\widetilde{t}_{int} = \widetilde{T}_{out} - \widetilde{T}_{in}$. Two distinct characteristic lengths, d_1 and d_2, represent the distance of penetration into the shock to reach the ramp and the overshoot and are sketched in (e).

forth between the upstream edge of the front and the overshoot several times before being finally reflected by the shock front (as illustrated by Figure 5d). Then important information can be deduced from these diagnostics based on both $\widetilde{L}_{\text{depth}}$ and $\Delta\widetilde{t}_{\text{int}}$ measurements as follows:

[32] 1. Concerning the interaction time range $\left(\Delta\widetilde{t}_{\text{int}}\right)$, Figures 5a–5c show discontinuous distributions of particles which form temporal "bursts." For example, the first "burst" (#1) of Figure 5a is localized around $1\widetilde{\tau}_{ci}$. This "burst" represents all ions which have freshly interacted with the shock front during the same time range. The time interval between each "burst" is $\approx 0.5\widetilde{\tau}_{ci}$ which corresponds to one half ion gyration in the upstream region.

[33] 2. Clearly, nearly all reflected ions spent their time within the shock front and do not cross the overshoot region. The interaction time range $\Delta\widetilde{t}_{\text{int}}$ is almost independent of the penetration depth $\widetilde{L}_{\text{depth}}$ which evidences that each "burst" represents a bounce against the shock front. More precisely, the first "burst" (#1) is formed by particles having suffered one bounce on the shock front, the second "burst" (#2) by particles having suffered two bounces on the shock front, and so on.

[34] 3. As shown in all plots of Figures 5a–5c, all multi-bounce particles stay in the same $\widetilde{L}_{\text{depth}}$ range defined by the two distances $\widetilde{d}_1 \approx \widetilde{\rho}_{ci}/2$ and $\widetilde{d}_2 \approx 2.5\widetilde{\rho}_{ci}$, respectively. Such distances allow us to define three distinct domains as illustrated by the Figure 5e. The first domain ($d \leq d_1$) corresponds to particles which stay in the foot and then do not reach the ramp. The second domain ($d_1 \leq d \leq d_2$) corresponds to ions which penetrate more deeply into the shock front moving back and forth between the upstream edge of the shock ramp and the overshoot (i.e., these particles interact with the ramp several times). The third domain ($d \geq d_2$) corresponds to ions which penetrate into the downstream region before succeeding to catch up with the shock front and to escape back upstream. Then these last ions can be considered as "leaking" from the downstream region and form a possible source of backstreaming ions. Nevertheless, in the present simulation, the number of "leaked" particles is very low, and no definitive conclusion can be drawn on the relative contribution of this particular population to the ion foreshock. Then we will focus only on the particles directly reflected at the shock front itself, i.e., on ions found in the range $0 \leq d \leq d_2$.

[35] 4. Applying this classification to Figures 5a–5c, we observe that only the first "burst" (named #1 with $\Delta\widetilde{t}_{\text{int}} \approx 1\widetilde{\tau}_{ci}$) is present in the $0 \leq \widetilde{L}_{\text{depth}} \leq \widetilde{d}_2$ domain. In other words, only particles suffering one bounce on the shock front are reflected either in the foot or at the ramp. By contrast, all multi-bounces reflected ions ("bursts" #2, #3, #4 and #5) belong to the $\widetilde{d}_1 \leq \widetilde{L}_{\text{depth}} \leq \widetilde{d}_2$ domains and then are reflected back at the ramp (where the electrostatic potential barrier is the highest) and never in the foot region.

[36] 5. Comparing Figures 5a–5c, the number of bounces strongly depends on the propagation angle θ_{Bn}. In Figure 5a, (i.e., pop 1 defined for $59° \leq \theta_{Bn} \leq 66°$), one can identify almost three bounces (i.e., three bursts named #1, #2, and #3) before the statistics becomes too low at later times $\left(\Delta\widetilde{t}_{\text{int}} > 2\widetilde{\tau}_{ci}\right)$. This box collects ions freshly reflected by the shock front (near the foreshock edge) and not many bounces are expected. In Figure 5b, (i.e., pop 2 defined for $52° \leq \theta_{Bn} < 59°$), the number of reflected particles is more important (we are in the angular range where a large number of ions are backstreaming), and we observe up to 4–5 bounces. Finally, in the last Figure 5d (i.e., pop 3 defined for $45° \leq \theta_{Bn} < 52°$), the number of bounces decreases to three since we are near the $\theta_{Bn} \approx 45°$ frontier which filters out those having more bounces (below this frontier, no particles are analyzed herein). At this stage, we have to point out that the exact number of bounces is not so important since it depends on the numerical statistics and can vary from one sampling box to the other. Nevertheless, more relevant is the decrease of the reflected ions density as the number of bounces increases. Indeed, statistics are more difficult for populations suffering four or more bounces (as evidenced in Figures 5a and 5b). Then most backstreaming particles gain enough energy after only one, two, or three bounces which demonstrate that the associated acceleration processes are very efficient.

[37] The analysis of these different features stresses the importance of the time range $\Delta\widetilde{t}_{\text{int}}$ and the penetration depth $\widetilde{L}_{\text{depth}}$ parameters to possibly identify the "FAB" and "GPB" populations. Indeed, $\Delta\widetilde{t}_{\text{int}}$ allows us to separate clearly the one bounce population from the multi-bounces population which is important since only gyrotropic population (i.e., "FAB") is expected to be associated with the multi-bounces. Indeed, during this long-time process $\left(\Delta\widetilde{t}_{\text{int}} > 1\widetilde{\tau}_{ci}\right)$, particles are coming from different places and angular regions of the curved shock front. In this way, they lose their gyrophase correlation (or more simply have initially independent gyrophase), and a gyrotropic pitch angle distribution is expected. On the other hand, gyrophase bunched distributions (i.e., "GPB") need to satisfy two important conditions: (i) only a small percentage of particles which penetrate the shock constitute the "GPB" population; otherwise, it should dominate everywhere in the ion foreshock which is not the case; and more important, (ii) particles have to be highly confined in the perpendicular velocity space to form a bunch. This last point requires a small interaction time range $\left(\Delta\widetilde{t}_{\text{int}} < 1\widetilde{\tau}_{ci}\right)$ with the shock front in order to preserve their gyrophase correlation. As evidenced in Figure 5, for small $\Delta\widetilde{t}_{\text{int}}$, ions can be reflected either in the foot or at the ramp depending on the value of the penetration depth $\widetilde{L}_{\text{depth}}$. Nevertheless, as described by *Gurgiolo et al.* [1981], the "GPB" population can be produced by a strong electrostatic field like the one observed in the ramp which seems to be a good candidate to create a non-gyrotropic population. In conclusion, the "GPB" population needs to satisfy simultaneously the two criteria—$\Delta\widetilde{t}_{\text{int}} < 1\widetilde{\tau}_{ci}$ and $\widetilde{L}_{\text{depth}} \geq \widetilde{d}_1$—whereas the "FAB" population does not satisfy $\Delta\widetilde{t}_{\text{int}} < 1\widetilde{\tau}_{ci}$.

[38] In order to check this scenario, Figures 6 and 7 plot the pitch angle distribution and the perpendicular velocity space of ions which follow the time and spatial criteria described above for the populations 2 and 3, respectively. Particles in the angular range $59° \leq \theta_{Bn} \leq 66°$ (population 1) are not plotted since these ions are gyrotropic in the perpendicular velocity space (Figure 2); in addition, the number of particles is too low to be considered as relevant from a statistical point of view when they are splitted

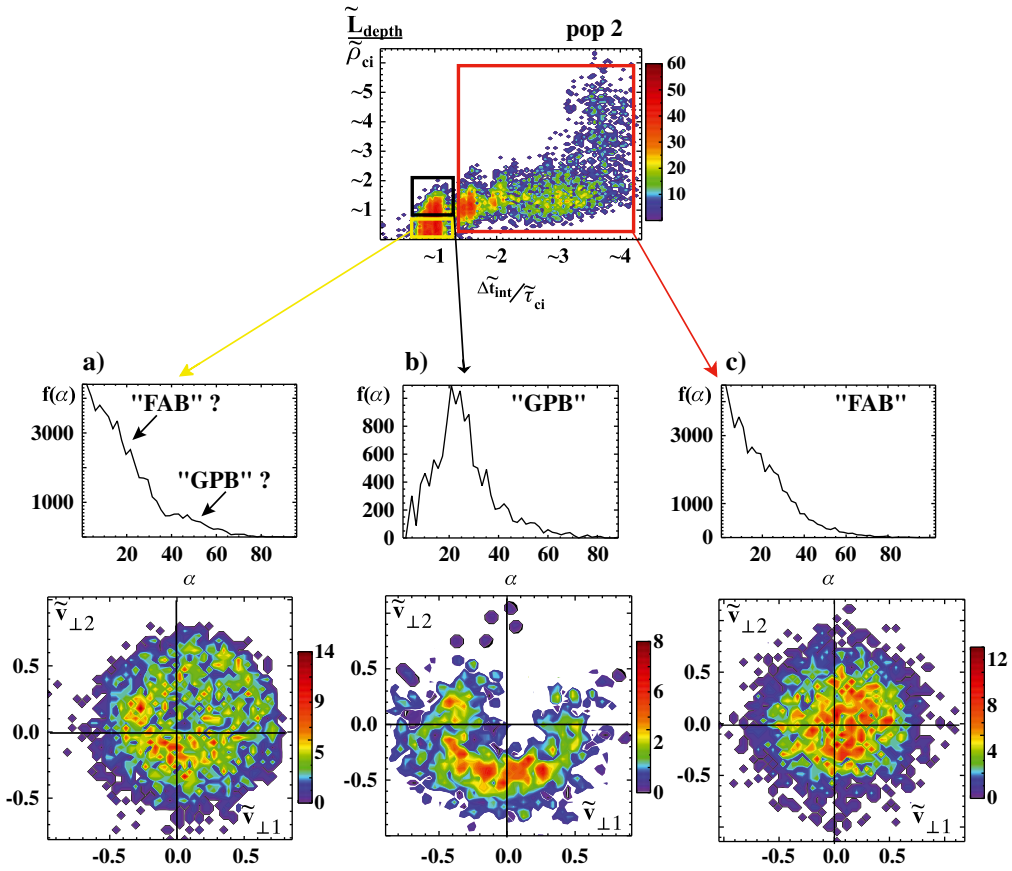

Figure 6. The population 2 is splitted into different sub-group after applying the two criteria $\widetilde{L}_{\mathrm{depth}}$ and $\Delta\widetilde{t}_{\mathrm{int}}$ as described in the text. The sub-group are represented by the thick line squares in the top panel used as a reference for the population 2 of Figure 5b. Local pitch angle distribution $f(\alpha)$ and perpendicular velocity distribution $(\widetilde{v}_{\perp 1}, \widetilde{v}_{\perp 2})$ are plotted for each group. Right panels (c) show a "FAB" population for $\Delta\widetilde{t}_{\mathrm{int}} > 1\widetilde{\tau}_{ci}$ and $\widetilde{L}_{\mathrm{depth}} > 1\widetilde{\rho}_{ci}$, while in middle panels (b) evidence a "GPB" population for $\Delta\widetilde{t}_{\mathrm{int}} < 1\widetilde{\tau}_{ci}$ and $\widetilde{L}_{\mathrm{depth}} > 1\widetilde{\rho}_{ci}$. Only the left panels (a) obtained for $\Delta\widetilde{t}_{\mathrm{int}} < 1\widetilde{\tau}_{ci}$ and $\widetilde{L}_{\mathrm{depth}} < 1\widetilde{\rho}_{ci}$ do not clearly separate the "FAB" and "GPB" populations.

into smaller groups. Then Figure 6 plots the three distinct sub-populations: (i) one with $\Delta\widetilde{t}_{\mathrm{int}} < 1\widetilde{\tau}_{ci}$ and $\widetilde{L}_{\mathrm{depth}} \leq \widetilde{d}_1$ (Figure 6a). This population is composed with ions which do not reach the ramp and are reflected back in the foot; (ii) one with $\Delta\widetilde{t}_{\mathrm{int}} < 1\widetilde{\tau}_{ci}$ and $\widetilde{d}_1 \leq \widetilde{L}_{\mathrm{depth}} \leq \widetilde{d}_2$ which concerns backstreaming ions reflected by the ramp after only one bounce (Figure 6b); and finally, (iii) one with $\Delta\widetilde{t}_{\mathrm{int}} > 1\widetilde{\tau}_{ci}$ and $\widetilde{d}_1 \leq \widetilde{L}_{\mathrm{depth}}$ populated by the multi-bounces reflected particles (Figure 6c). These new criteria allow us to discriminate more clearly between "FAB" and "GPB" populations. In agreement with the expected results, Figure 6b shows a non-gyrotropic distribution (i.e., "GPB" population) with a pitch angle around $\alpha \approx 25°$, while Figure 6c shows a characteristic gyrotropic distribution (i.e., "FAB" population) with a pitch angle $\alpha \approx 0°$. It is only difficult to conclude for the Figure 6a where both perpendicular velocity and pitch angle distributions still show mixed features of both populations. Indeed, in this figure, we observe a pitch angle distribution with a maximum for $\alpha \approx 0°$ characteristic of the "FAB" population. Nevertheless, the tail of the same distribution shows a small bump around $\alpha \approx 45°$ which could be associated to a "GBP" population. At the present time, this case requires further investigation and is out of the scope of this paper. Figure 7 recovers similar results; i.e., the "GPB" population is clearly evidenced for particles reflected by the ramp after only one bounce (Figure 7a) and the "FAB" for ions which have suffered almost two bounces on the ramp (Figure 7b).

[39] In summary, we observe the "FAB" population when reflected ions have undergone several bounces at the shock ramp, and "GPB" population among particles which have interacted only once with the ramp. Obviously, the main consequence is that the "FAB" ions are more numerous than the "GPB" ions and overwhelm these in the measurement of the local perpendicular velocity distribution. Present results allow us to understand more clearly the difficulties encountered to analyze Figure 2 in order to separate "FAB" and "GPB" populations. These new criteria have to be used in order to recover the usual scheme proposed in Figure 3 (section 3.3).

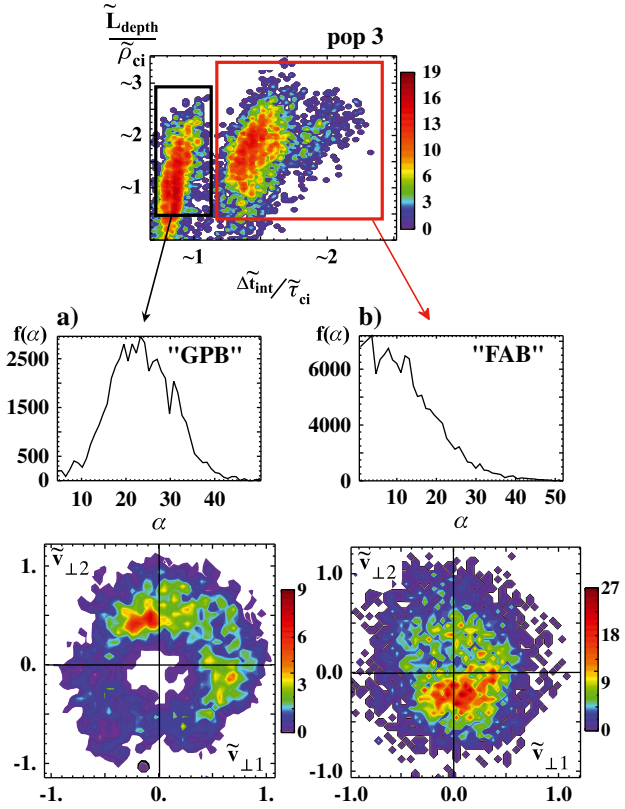

Figure 7. Similar to Figure 6 but for the population 3 (i.e., far from the shock front and in the $45° \leq \theta_{Bn} < 52°$ range). Only two groups, namely defined for $\left(\Delta\widetilde{t}_{\rm int} > 1\tau_{ci}, \widetilde{L}_{\rm depth} > 1\widetilde{\rho}_{ci}\right)$ for the left panels ("GPB" population) and for $\left(\Delta\widetilde{t}_{\rm int} < 1\widetilde{\tau}_{ci}, \widetilde{L}_{\rm depth} > 1\widetilde{\rho}_{ci}\right)$ for the right panels ("FAB" population), have been identified.

5. Conclusions

[40] To the knowledge of the authors, it is the first time that the ion foreshock has been retrieved in a 2-D PIC self-consistent simulation. The present simulation is restricted to the quasi-perpendicular angular domain. The ion foreshock is identified within a certain angular range ($45° \leq \theta_{Bn} \leq 66°$) where after interacting with the shock front, some ions do have the appropriate parallel velocity (larger than the parallel shock front velocity) to escape into the solar wind. It is also the first time that both backstreaming "FAB" and "GPB" ion populations are observed simultaneously in 2-D PIC simulations.

[41] The use of 2-D PIC simulations is justified for two main reasons: (i) to analyze the origin of FAB and GPB populations in the case where the detailed structures of the shock front are fully involved self-consistently; the reflection mechanisms are not reduced to simple specular reflection only but involve more intricate processes as those responsible for multi-bounces; (ii) the electron foreshock has been also retrieved in our present simulations and has been analyzed in previous works (but is not developed in the present study dedicated to the ion foreshock only). Then the mutual interaction of both foreshocks is made possible but is left for further work; (iii) and last but not least, PIC simulations present the advantage of including self-consistently small-scale fluctuations along the shock front [*Savoini and Lembege*, 1994; *Savoini and Lembege*, 2001] and along the shock normal [*Muschietti and Lembege*, 2006; *Matsukiyo and Scholer*, 2003, 2006] where electrons dynamics is included. All these works were performed for planar shock fronts only. Such small-scale fluctuations are also expected in a curved shock front and could have a possible impact on the ion reflection processes, but have not been analyzed, yet.

[42] In addition, "FAB" population coming from the downstream region is observed as suggested in certain studies [*Thomsen et al.*, 1983a], whereas recent papers claim that the ion "leakage" is unlikely [*Kucharek et al.*, 2004; *Oka et al.*, 2005. Nevertheless, the study of this particular "FAB" population is out of scope of the present paper because the number of these "leaked" ions is very low to be statistically relevant and a larger number of particles per cell must be used.

[43] In any case, present simulations have emphasized that the typical gyrotropic/non-gyrotropic features and the pitch angle distribution commonly used in the literature are not fully appropriate near the shock front where both populations cannot be clearly separated. Indeed, present results stress that larger distances upstream from the shock front are in favor for separating more clearly "FAB" and "GPB" populations. At short distance, this separation is more difficult and requires the use of two new additional criteria—namely, the interaction time range $\left(\Delta\widetilde{t}_{\rm int}\right)$ and the penetration depth

$\left(\widetilde{L}_{\text{depth}}\right)$ into the shock front—to separate more clearly the "FAB" and "GPB" populations. The main features of both backstreaming ion populations can be summarized as follows:

[44] **"FAB population":** This population is observed near the edge of the ion foreshock, persists even far from the shock front, and is dominant near the shock front whatever the angle is within $45° \leq \theta_{Bn} \leq 66°$ range. It represents about 85% of the whole backstreaming particles. Results show that if the shock front is the source of this particular population, several origins may be invoked depending on the interaction time and the angular domain of propagation θ_{Bn}. This dependency requires a time trajectories analysis of individual particles which is under active investigation, but some information can be already deduced. The "FAB" population is observed both for short $\left(\Delta\widetilde{t}_{\text{int}} < 1\widetilde{\tau}_{ci}\right)$ and long $\left(1\widetilde{\tau}_{ci} \leq \Delta\widetilde{t}_{\text{int}} \leq 4\widetilde{\tau}_{ci}\right)$ interaction time range. Nevertheless, the main source of the "FAB" is associated to long-time interactions where particles move back and forth between the upstream edge of the front and the overshoot $\left(\widetilde{d}_1 \leq \widetilde{L}_{\text{depth}} \leq \widetilde{d}_2\right)$. These ions suffer an acceleration by the convective electric field along the shock front until they succeed to gain enough energy to escape into the upstream region. Figure 5 shows us that this acceleration process is neither uniform nor continuous at the shock front but has discrete time sub-ranges corresponding to the formation of ion "bursts." These bursts illustrate the ion cyclotron motion during its drift along the curved shock front and are separated by an half gyroperiod $\widetilde{T}_{\text{drift}} \approx 1/2\widetilde{\tau}_{ci}$ which corresponds to the half gyration covered by the reflected ions traveling along the curved shock front. As a consequence, the "FAB" ions are not reflected back upstream at the same time and at the same place ("time-of-flight" effects are included self-consistently) and therefore do not see the same shock front structures. Then these form a gyrotropic perpendicular velocity distribution (i.e., no phase correlation).

[45] **"GPB population":** This second population presents distinct properties in terms of both pitch angles and of spatial distribution within the foreshock region. In contrast with the "FAB" population, its origin has to satisfy two restrictive conditions: (i) incoming ions have to reach the potential barrier of the front where the electrostatic field is stronger (no foot reflection), and (ii) they must gain enough energy to escape upstream only after one bounce on the shock front; otherwise, they lose their phase correlation and cannot form the characteristic velocity bunched distribution as already described by *Gurgiolo et al.* [1981]. This last condition explains why "GPB" populations appear more deeply in the foreshock, for lower propagation angle θ_{Bn} where escaping conditions are easier for the same parallel acceleration efficiency. Likewise, another consequence is that the number of "GPB" ions is lower than the "FAB" ions. Then "GPB" population is embedded within the "FAB" population near the shock front which explains the difficulty to identify such population in the experimental data. The use of two additional parameters $\Delta\widetilde{t}_{\text{int}}$ and $\widetilde{L}_{\text{depth}}$ is necessary to separate clearly both populations and to recover the respective well-known characteristics illustrated in Figure 3.

[46] Nevertheless, at this stage, let us remind that the spatial extension of the ion foreshock in our simulation is presently artificially limited by CPU and RAM computational constraints to only $130c/\omega_{pi}$ ($\sim 2R_E$ with the standard values of the solar wind). Then other mechanisms are possible to explain the generation of the non-gyrotropic population which cannot be included in our simulation. Let us precise that our scenario does not suppress the possibility that ion instabilities may have some impact on ion dynamics and on resulting local ion distribution functions at large upstream distance from the curved shock front. In particular, a large amount of works has been already done on beam-plasma instabilities which can interact with the "FAB" and convert these into "GPB" populations [*Hoshino and Terasawa*, 1985; *Mazelle et al.*, 2003; *Meziane*, 2005; *Mazelle et al.*, 2005; *Kis et al.*, 2007]. Such "FAB" distributions are observed in association with low-frequency quasi-monochromatic waves with large amplitudes ($\delta B/B \sim 1$). The properties of the ULF waves reveal that these are in cyclotron resonance with the ion parallel beams that could drive a right-hand ion/ion instability responsible for the wave occurrence [*Mazelle et al.*, 2003]. Then it is commonly claimed that non-gyrotropic ions are obtained locally (e.g., far from the shock front, at larger distances $\sim 10R_E$) and result from the disruption of the "FAB" population [*Meziane et al.*, 1997, 2001, 2004a; *Meziane*, 2005; *Mazelle et al.*, 2003].

[47] In conclusion, present numerical results are qualitatively in good agreement with the experimental data [*Fuselier et al.*, 1986a; *Meziane et al.*, 2005] for both "FAB" and "GPB" populations. More important, regardless of the concerned reflection process, our simulation demonstrates that both "FAB" and "GPB" populations can be produced by the macroscopic fields at the shock front. No local wave activity and related pitch angle scattering mechanism need be invoked to put reflected ions into the regions of velocity space directly accessible to the upstream region [*Möbius et al.*, 2001; *Kucharek et al.*, 2004]. In other words, "FAB" can be produced by multiple reflections at the shock front like the well-known proposed shock surfing acceleration (SSA) process described in *Shapiro and Üçer* [2003] and *Yang et al*. [2009, 2012]. In complement to these previous works based on planar shock front, let us remind that a curved shock is concerned here. On the other hand, if one considers the mechanisms proposed in the literature for the production of the "GPB" ions, it is appropriate to emphasize the leading role of the electrostatic field present at the ramp as discussed by *Gurgiolo et al*. [1981, 1983] in order to explain their formation in our simulation. In fact, the "GPB" population suggests that strong temporal variations exist within the shock front. Then the shock front acts in time to create bunched distributions from the gyrotropic upstream ion distribution. In other words, the "GPB" ions cannot be produced from a long-time process as multi-bounces acceleration which imposes a phase-mixing inconsistent with this population. A bursty process associated to the shock front non-stationarity such as the shock front self-reformation [*Lembege and Dawson*, 1987; *Lembege and Savoini*, 1992] can be proposed in order to launch "packets" of ions [*Gurgiolo et al.*, 1983; *Motschmann et al.*, 1999]. This scenario and the acceleration processes involved in the formation of "FAB" and "GPB" populations must

be confirmed later on by the analysis of the individual particle trajectories.

[48] **Acknowledgments.** Simulation runs have been performed on the *SX*8 machine of the supercomputer center IDRIS located at Orsay (near Paris). Thanks must be addressed to Jean-Noel Leboeuf for having provided the basic (periodic) version of the 2-D code.

References

Bale, S., et al. (2005), Quasi-perpendicular shock structure and processes, *Space Sci. Rev.*, *118*, 161–203, doi:10.1007/s11214-005-3827-0.

Blanco-Cano, X., N. Omidi, and C. Russell (2006a), Macrostructure of collisionless bow shocks: 2. ULF waves in the foreshock and magnetosheath, *J. Geophys. Res.*, *111*, A10,205, doi:10.1029/2005JA011421.

Blanco-Cano, X., N. Omidi, and C. Russell (2006b), ULF waves and their influence on bow shock and magnetosheath structures, *Adv. Space Res.*, *37*, 1522–1531, doi:10.1016/j.asr.2005.10.043.

Blanco-Cano, X., N. Omidi, and C. Russell (2009), Global hybrid simulations: Foreshock waves and cavitons under radial interplanetary magnetic field geometry, *J. Geophys. Res.*, *114*, 01,216, doi:10.1029/2008JA013406.

Bonifazi, C., and G. Moreno (1981a), Reflected and diffuse ions backstreaming from the Earth's bow shock: 2. Origin, *J. Geophys. Res.*, *86* (A6), 4405–4413.

Bonifazi, C., and G. Moreno (1981b), Reflected and diffuse ions backstreaming from the Earth's bow shock. I. Basic properties, *J. Geophys. Res.*, *86*(A6), 4397–4404.

Constantinescu, O. D., K. Glassmeier, P. Décréau, and M. Fränz (2007), Low frequency wave sources in the outer magnetosphere, magnetosheath, and near Earth solar wind, *Ann. Geophys.*, *25*, 2217–2228, doi:10.5194/angeo.25-227-2007.

Eastwood, J., E. Lucek, C. Mazelle, and K. Meziane (2005), The foreshock, *Space Sci. Rev.*, *118*, 41–94, doi:10.1007/s11214-005-3824-3.

Edmiston, J. P., C. F. Kennel, and D. Eichler (1982), Escape of heated ions upstream of quasi-parallel shocks, *Geophys. Res. Lett.*, *9*(5), 531–534, doi:10.1029/GL009i005p00531.

Fuselier, S. (1995), Ion distributions in the Earth's foreshock upstream from the bow shock, *Adv. Space Res.*, *15*(8/9), 43–52.

Fuselier, S., M. Thomsen, and J. Gosling (1986a), Gyrating and intermediate ion distributions upstream from the Earth's bow shock, *J. Geophys. Res.*, *91*(A1), 91–99.

Fuselier, S., M. Thomsen, S. Gary, and S. Bame (1986b), The phase relationship between gyrophase-bunched ions and MHD-like waves, *Geophys. Res. Lett.*, *13*(1), 60–63.

Gary, S. P. (1981), Microinstabilities upstream of the Earth's bow shock—A brief review, *J. Geophys. Res.*, *86*, 4331–4336, doi:10.1029/JA086iA06p04331.

Gary, S. P., J. T. Gosling, and D. W. Forslund (1981), The electromagnetic ion beam instability upstream of the Earth's bow shock, *J. Geophys. Res.*, *86*(A8), 6691–6696, doi:10.1029/JA086iA08p06691.

Giacalone, J., J. R. Jokipii, and J. Kota (1994), Ion injection and acceleration at quasi-perpendicular shocks, *J. Geophys. Res.*, *99* (A10), 19-351–19-358.

Gosling, J. T., M. F. Thomsenn, S. J. Bame, W. C. Feldman, G. Pashmann, and N. Sckopke (1982), Evidence for specularly reflected ions upstream from the quasi-parallel bow shock, *Geophys. Res. Lett.*, *9*, 1333–1336.

Gurgiolo, C., G. K. Parks, B. H. Mauk, K. A. Anderson, R. P. Lin, H. Reme, and C. S. Lin (1981), Non-E x B ordered ion beams upstream of the Earth's bow shock, *J. Geophys. Res.*, *86*(A6), 4415–4424, doi:10.1029/JA086iA06p04415.

Gurgiolo, C., G. Parks, and G. Mauk (1983), Upstream gyrophase bunched ions—A mechanism for creation at the bow shock and the growth of velocity space structure through gyrophase mixing, *J. Geophys. Res.*, *88* (A11), 9093–9100.

Hada, T., M. Oonishi, B. Lembege, and P. Savoini (2003), Shock front nonstationarity of supercritical perpendicular shocks, *J. Geophys. Res.*, *108* (A6), 1233, doi:10.1029/2002JA009339.

Hamza, A. M., K. Meziane, and C. Mazelle (2006), Oblique propagation and nonlinear wave particle processes, *J. Geophys. Res.*, *111*, 04,104, doi:10.1029/2005JA011410.

Hellinger, P., P. Travnicek, and H. Matsumoto (2002), Reformation of perpendicular shocks: Hybrid simulations, *Geophys. Res. Lett.*, *29*(24), 2234, doi:10.1029/2002GL015915.

Hoppe, M. M., C. T. Russell, T. E. Eastman, and L. A. Frank (1982), Characteristics of the ULF waves associated with upstream ion beams, *J. Geophys. Res.*, *87*, 643, doi:10.1029/JA087iA02p00643.

Horbury, T. S., E. A. Lucek, A. Balogh, M. W. Dunlop, T. M. Oddy, C. Carr, P. Brown, A. Szabo, and K.-H. Fornacon (2001), Cluster magnetic field observations of the bowshock: Orientation, motion and structure, *Ann. Geophys.*, *19*, 1399–1409.

Hoshino, M., and T. Terasawa (1985), Numerical study of the upstream wave excitation mechanism. I. Nonlinear phase bunching of beam ions, *J. Geophys. Res.*, *90*(A1), 57–64.

Kis, A., M. Scholer, B. Klecker, E. Möbius, E. A. Lucek, H. Reme, J. M. Bosqued, L. M. Kistler, and H. Kucharek (2004), Multi-spacecraft observations of diffuse ions upstream of Earth's bow shock, *Geophys. Res. Lett.*, *31*(2), 20,801, doi:10.1029/2004GL020759.

Kis, A., M. Scholer, B. Klecker, H. Kucharek, E. A. Lucek, and H. Rème (2007), Scattering of field-aligned beam ions upstream of Earth's bow shock, *Ann. Geophys.*, *25*, 785–799, doi:10.5194/angeo-25-785-2007.

Kucharek, H. (2008), On the physics of collisionless shocks: Cluster investigations and simulations, *J. Atmos. Sol.-Terr. Phy.*, *70*, 316–324, doi:10.1016/j.jastp.2007.08.052.

Kucharek, H., and M. Scholer (1991), Origin of diffuse superthermal ions at quasi-parallel supercritical collisionless shocks, *J. Geophys. Res.*, *96*, 21,195–21,205.

Kucharek, H., E. Möbius, M. Scholer, C. Mouikis, L. Kistler, T. Horbury, A. Balogh, H. Réme, and J. Bosqued (2004), On the origin of field-aligned beams at the quasi-perpendicular bow shock: Multi-spacecraft observations by Cluster, *Ann. Geophys.*, *22*, 2301–2308, doi:10.5194/angeo-22-2301-2004.

Kuncic, Z., I. Cairns, and S. Knock (2004), A Quantitative model for terrestrial foreshock radio emissions: 1. Predicted properties, *J. Geophys. Res.*, *109*, A022,108, doi:10.1029/2003JA010125.

Lefebvre, B., Y. Seki, S. J. Schwartz, C. Mazelle, and E. A. Lucek (2010), Reformation of an oblique shock observed by Cluster, *J. Geophys. Res.*, *physics.space-ph*, 11,107, doi:10.1029/2009JA014268.

Lembege, B., and J. M. Dawson (1987), Self-consistent study of a perpendicular collisionless and nonresistive shock, *Phys. Fluids*, *30*, 1767, doi:10.1063/1.866191.

Lembege, B., and P. Savoini (1992), Nonstationarity of a two-dimensional quasiperpendicular supercritical collisionless shock by self-reformation, *Phys. Fluids*, *4*(11), 3533–3548.

Matsukiyo, S., and M. Scholer (2003), Modified two-stream instability in the foot of high Mach Number quasi-perpendicular shocks, *J. Geophys. Res.*, *108*(A12), 1459, doi: 10.1029/2003JA010080.

Matsukiyo, S., and M. Scholer (2006), On reformation of quasi-perpendicular collisionless shocks, *Adv. Space Res.*, *38*, 57–63, doi:10.1016/j.asr.2004.08.012.

Mazelle, C., et al. (2003), Production of gyrating ions from nonlinear wave-particle interaction upstream from the Earth's bow shock: A case study from Cluster-CIS, *Planet. Space Sc.*, *51*, 785–795, doi:10.1016/S0032-0633(03)00107-7.

Mazelle, C., K. Meziane, and M. Wilber (2005), Field-aligned and gyrating ion beams in a planetary foreshock, *AIP Conf. Proc.*, *781*, 89–94, doi:10.1063/1.2032680.

Mazelle, C., et al. (2010), SelfReformation of the QuasiPerpendicular Shock: CLUSTER Observations, *AIP Conf. Proc.*, *1216*, 471, doi:10.1063/1.3395905.

Meziane, K., M. Wilber, C. Mazelle, G. K. Parks, and A. M. Hamza (2005), A review of field-aligned beams observed upstream of the bow shock, *AIP Conf. Proc.*, *781*, 116–122, doi:10.1063/1.2032683.

Meziane, K., et al. (1997), Wind observation of gyrating-like ion distributions and low frequency waves upstream from the Earth's bow shock, *Adv. Space Res.*, *20*(4/5), 703–706, doi: 10.1016/S0273-1177(97)00459-6.

Meziane, K., C. Mazelle, R. P. Lin, D. Lequéau, D. E. Larson, G. K. Parks, and R. P. Lepping (2001), Three-dimensional observations of gyrating ion distributions far upstream from the Earth's bow shock and their association with low-frequency waves, *J. Geophys. Res.*, *106*(A4), 5731–5742, doi:10.1029/2000JA900079.

Meziane, K., et al. (2004a), Bow shock specularly reflected ions in the presence of low-frequency electromagnetic waves: A case study, *Ann. Geophys.*, *22*, 2325–2335, doi:10.5194/angeo-22-2325-2004.

Meziane, K., et al. (2004b), Simultaneous observations of field-aligned beams and gyrating ions in the terrestrial foreshock, *J. Geophys. Res.*, *109*, A05,107, doi:10.1029/2003JA010374.

Meziane, K., M. Wilber, A. M. Hamza, C. Mazelle, G. K. Parks, H. Rème, and E. A. Lucek (2007), Evidence for a high-energy tail associated with foreshock field-aligned beams, *J. Geophys. Res.*, *112*, A01,101, doi:10.1029/2006JA011751.

Möbius, E., et al. (2001), Observations of the spatial and temporal structure of field-aligned beam and gyrating ring distributions at the quasi-perpendicular bow shock with Cluster CIS, *Ann. Geophys.*, *19*, 1411.

Motschmann, U., K. Glassmeier, and A. Brinca (1999), Nongyrotropic particle distributions in space plasmas, *Ann. Geophys.*, *17*, 613–622.

Muschietti, L., and B. Lembege (2006), Electron cyclotron microinstability in the foot of perpendicular shock: A self-consistent PIC simulation, *Adv. Space Res.*, *37*, 483–493, doi: 10.1016/j.asr.2005.03.077.

Oka, M., T. Terasawa, Y. Saito, and T. Mukai (2005), Field-aligned beam observations at the quasi-perpendicular bow shock: Generation and shock angle dependence, *J. Geophys. Res.*, *110*, 05,101, doi:10.1029/2004JA010688.

Omidi, N., X. Blanco-Cano, and C. T. Russell (2005), Macrostructure of collisionless bow shocks: 1. Scale lengths, *J. Geophys. Res.*, *110*, A12,212, doi:10.1029/2005JA011169.

Omidi, N., X. Blanco-Cano, and C. Russell (2006), Global hybrid simulations of solar wind interaction with Mercury: Magnetosperic boundaries, *Adv. Space Res.*, *38*, 632–638, doi:10.1016/j.asr.2005.11.019.

Paschmann, G., N. Sckopke, and J. Asbridge (1980), Energization of solar wind ions by reflection from the Earth's bow shock, *J. Geophys. Res.*, *85* (A9), 4689–4693.

Paschmann, G., N. Sckopke, J. R. Asbridge, S. J. Bame, and J. T. Gosling (1981), Characteristics of reflected and diffuse ions upstream from the Earth'bow shock, *J. Geophys. Res.*, *86*, 4355–4364.

Přech, L., J. Šafránková, Z. Němeček, and K. Kudela (2005), INTERBALL-1 observations of plasma and energetic particle fluxes upstream of the Earth's bow shock, *Planet. Space Sc.*, *53*, 65–78, doi: 10.1016/j.pss.2004.09.030.

Savoini, P., and B. Lembege (1994), Electron dynamics in two- and one-dimensional oblique supercritical collisionless magnetosonic shocks, *J. Geophys. Res.*, *99*(A4), 6609–6635

Savoini, P., and B. Lembège (1999), Full curvature effects of a collisionless shock, *Adv. Space Res.*, *24*, 13–22.

Savoini, P., and B. Lembège (2001), Two-dimensional simulations of a curved shock: Self-consistent formation of the electron foreshock, *J. Geophys. Res.*, *106*, 12,975, doi:10.1029/2001JA900007.

Savoini, P., B. Lembege, and J. Stienlet (2010), Origin of backstreaming electrons within the quasi-perpendicular foreshock region: Two-dimensional self-consistent, PIC simulation, *J. Geophys. Res.*, *115*(A9), A09,104, doi:10.1029/2010JA015263.

Scholer, M., and S. Matsukiyo (2004), Nonstationarity of quasi-perpendicular shocks: A comparison of full particle simulations with different ion to electron mass ratio, *Ann. Geophys.*, *22*, 2345–2353, doi: 10.5194/angeo-22-2345-2004.

Schwartz, S. J., and D. Burgess (1984), On the theoretical/observational comparison of field-aligned ion beams in the earth's foreshock, *J. Geophys. Res.*, *89*, 2381–2384, doi:10.1029/JA089iA04p02381.

Schwartz, S. J., M. F. Thomsen, and J. T. Gosling (1983), Ions upstream of the earth's bow shock—A theoretical comparison of alternative source populations, *J. Geophys. Res.*, *88* (A3), 2039–2047, doi:10.1029/JA088iA03p02039.

Shapiro, V. D., and D. Üçer (2003), Shock surfing acceleration, *Planet. Space Sc.*, *51*, 665–680, doi:10.1016/S0032-0633(03)00102-8.

Shin, K., H. Kojima, H. Matsumoto, and T. Mukai (2008), Characteristics of electrostatic solitary waves in the Earth's foreshock region: Geotail observations, *J. Geophys. Res.*, *113*, A03,101, doi: 10.1029/2007JA012344.

Sibeck, D. G., N. Omidi, I. Dandouras, and E. Lucek (2008), On the edge of the foreshock: Model-data comparisons, *Ann. Geophys.*, *26*, 1539–1544, doi:10.5194/angeo-26-1539-2008.

Sonnerup, B. U. Ö. (1969), Acceleration of particles reflected at a shock front, *J. Geophys. Res.*, *74*(5), 1301–1304, doi:10.1029/JA074 i005p01301.

Tanaka, M., C. C. Goodrich, D. Winske, and K. Papadopoulos (1983), A source of the backstreaming ion beams in the foreshock region, *J. Geophys. Res.*, *88*(A4), 3046–3054, doi:10.1029/JA088iA04p03046.

Thomas, V. A., and D. Winske (1990), Two dimensional hybrid simulation of a curved bow shock, *Geophys. Res. Lett.*, *17*(9), 1247–1250, doi:10.1029/GL017i009p01247.

Thomsen, M., J. Gosling, and S. Bame (1985), Gyrating ions and large-amplitude monochromatic MHD waves upstream of the Earth's bow shock, *J. Geophys. Res.*, *90*(A1), 267–273.

Thomsen, M. F., J. T. Gosling, S. J. Bame, W. C. Feldman, G. Paschmann, and N. Sckopke (1983a), Field-aligned ion beams upstream of the earth's bow shock: Evidence for a magnetosheath source, *Geophys. Res. Lett.*, *10*(12), 1207–1210, doi:10.1029/GL010i012p01207.

Thomsen, M. F., J. T. Gosling, and S. J. Schwartz (1983b), Observational evidence on the origin of ions upstream of the earth's bow shock, *J. Geophys. Res.*, *88*(A10), 7843–7852, doi:10.1029/JA088iA10p07843.

Tsurutani, B. T., and P. Rodriguez (1981), Upstream waves and particles—An overview of ISEE results, *J. Geophys. Res.*, *86*, 4317–4324.

Winske, D., and M. M. Leroy (1984), Diffuse ions produced by electromagnetic ion beam instabilities, *J. Geophys. Res.*, *89*, 2673–2688.

Yang, Z. W., Q. M. Lu, B. Lembège, and S. Wang (2009), Shock front nonstationarity and ion acceleration in supercritical perpendicular shocks, *J. Geophys. Res.*, *114*, 03,111, doi:10.1029/2008JA013785.

Yang, Z. W., B. Lembege, and Q. M. Lu (2012), Impact of the rippling of a perpendicular shock front on ion dynamics, *J. Geophys. Res.*, *117*(A7), A07,222, doi:10.1029/2011JA017211.